

Automatic Bilateral Symmetry (Midsagittal) Plane Extraction from Pathological 3D Neuroradiological Images

Yanxi Liu^a, Robert T. Collins^a and William E. Rothfus^b

^aThe Robotics Institute, Carnegie Mellon University, 5000 Forbes Ave.,
Pittsburgh, PA 15213, USA

^bRadiologic Sciences, Diagnostic Radiology, Allegheny University of the
Health Sciences (Allegheny General Hospital), Pittsburgh, USA

ABSTRACT

Most pathologies (tumor, bleed, stroke) of the human brain can be determined by a symmetry-based analysis of neural scans showing the brain's 3D internal structure. Detecting departures of this internal structure from its normal bilateral symmetry can guide the classification of abnormalities. This process is facilitated by first locating the ideal symmetry plane (midsagittal) with respect to which the brain is invariant under reflection. An algorithm to automatically identify this bilateral symmetry plane from a given 3D clinical image has been developed. The method has been tested on both normal and pathological brain scans, multimodal data (CT and MR), and on coarsely sliced samples with elongated voxel sizes.

Keywords: bilateral symmetry, midsagittal plane, cross-correlation

1. INTRODUCTION

Normal human brains present an approximate bilateral symmetry with respect to their midsagittal planes, this symmetry is often absent in pathological brains. Most pathologies (tumor, bleed, stroke) of the human brain can be determined by a symmetry-based analysis of neural scans showing the brain's 3D internal structure (Figure 1). Such asymmetries are caused either by *mass effect*, which is the displacement of anatomical structures away from their normal positions, or by a density imbalance due to lesion in or around the brain. Detecting departures of this internal structure from its normal bilateral symmetry can guide the classification of abnormalities. This process is facilitated by first locating the ideal symmetry plane (midsagittal) with respect to which the brain is invariant under reflection. The bilateral symmetry of the brain is easily seen in CT and MR images depicting axial and coronal slices (Figure 1). However, automatic extraction of the 3D plane of bilateral symmetry is difficult due to a number of factors. First, there is no enforced standard among technicians when taking brain scans. Each set of slices may differ from other sets in the angle of scanning, the start and end positions of the scan, the distance between adjacent slices, and the total number of slices. Second, the patient's head may be tilted during the scanning process or moved midway, resulting in a set of slices on which the brain does not appear to be perfectly symmetrical. Third, the human skull and brain are only approximately symmetric – asymmetries such as air pockets and the presence of lesions must be ignored when computing the axis of symmetry, so that window-based or segmentation-based approaches¹ are likely to fail. Fourth, clinical brain slice images sometimes contain background clutter in the form of patient data superimposed directly on the image, which must be ignored. And finally, clinical brain scans typically consist of coarsely-spaced slices with elongated voxel sizes (e.g. voxel sizes of 1:1:20 (mm^3)) and with only a subportion of the brain visible in the set of scans. Table 1 shows the parameters of a few sample input image sets. Due to the fact that the voxels of some 3D images can be far from cubical, the algorithm described here is a pixel-based instead of voxel-based 3D image algorithm. Unlike the finely sampled research data containing the entire brain used by most neurological image understanding researchers, this kind of input makes it difficult to infer 3D structure by interpolating the missing data between slices. Studying algorithms that deal with real clinical images originates from our desire to facilitate on-line clinical image indexing and retrieval for real-time medical consultation.⁶

We have developed a simple yet robust algorithm that can extract the bilateral symmetry plane of a brain from a set of clinical CT or MR images, regardless of coarse spacing or partial sampling, background clutter, asymmetries

Send correspondence to Dr. Yanxi Liu: E-mail: yanxi@cs.cmu.edu,
URL: http://www.cs.cmu.edu/yanxi/www/images/medical_image.html

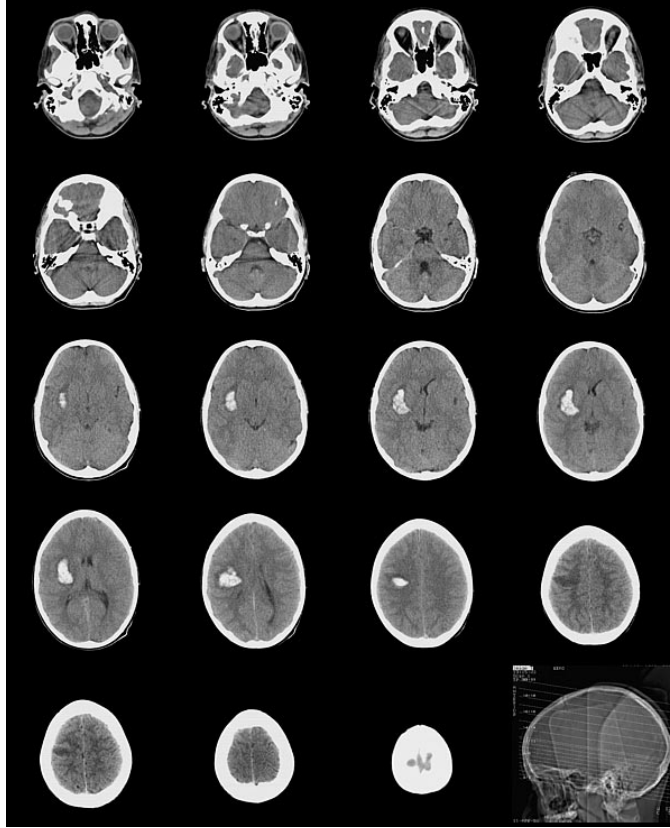


Figure 1. A typical set of clinical CT scans (axial), only captures a portion of a patient’s head, as shown in a side view on the lower right corner. This is a case of acute right basal ganglion bleed.

of the skull, presence of mass effect and brain pathologies such as tumors, bleeds or stroke. The rotation errors existing in the image can be up to ± 90 degrees. The results agree to within one degree of rotation with those achieved by a human expert. In contrast to most current symmetry detection algorithms^{4,8,16,18} the symmetry plane/axis is not simply extracted where it appears (for normal brains) but where *it is supposed to be* (for pathological brains). Although maximization of mutual information theory has been applied successfully for multimodality brain registrations under rigid and sometimes affine transformations^{7,12,15,17} we have not found it capable of extracting the ideal symmetry plane for pathological brain data, which can exhibit severe asymmetries. In Section 2 we present the underlying geometry of our new symmetry extraction algorithm (Section 2.1), the algorithmic steps (Section 2.2), and experiment results and evaluations (Section 2.3). Section 3 concludes the paper with a brief summary and future work.

2. 3D BILATERAL SYMMETRY PLANE EXTRACTION

Neuroradiology scans are in nature 3D volumetric data expressed as a stack of 2D images. In this section we present a geometric analysis and working algorithm for extracting the brain’s 3D bilateral symmetry plane from this set of 2D image slices.

We define an *ideal head coordinate system* centered in the brain with positive X_0, Y_0 and Z_0 axes pointing in the right, anterior and superior directions respectively (Figure 2, white coordinate axes).¹³ With respect to this coordinate system, the *bilateral symmetry plane* of the brain is defined as the plane $X_0 = 0$. This plane is often referred to as the *mid-sagittal* plane of the brain. Ideally, a set of *axial (coronal)* slices is cut perpendicular to the $Z_0(Y_0)$ axis, and the intersection of each slice with the bilateral symmetry plane appears as a vertical line on the slice*. In clinical practice, due to various positioning errors, we are presented not with the ideal coordinate system,

*The analysis given to the axial slices from now on can be applied to coronal slices (cut along the Y axis) as well with corresponding symbols changed: ‘Z’ to ‘Y’.

Table 1. A Subset of Input 3D Image Data

Set	Modality	#Slices	Form and Size	Voxel (mm)	Pathology
1	CT	18	axial 664x534	0.5x0.5x2 (1-10) 0.5x0.5x10 (11-18)	Right occipital/parietal acute bleed
2	CT	19	axial 524x518	0.5x0.5x5 (1-11) 0.5x0.5x10 (12-19)	Basal ganglion acute bleed
3	CT enhanced	33	axial 686x550	0.5x0.5x5 (1-15) 0.5x0.5x10 (16 - 33)	right parietal/occipital meningioma
4	MR	187	axial 176x236	0.98x0.98x1.2	Normal
5	MR (T1)	123	coronal 256x256	0.9375x0.9375x1.5	Atlas, Normal
6	CT	16	axial 686x550	0.5x0.5x10	Basal ganglion acute bleed
7	CT	9	axial 686x550	0.5x0.5x10	Right thalamic acute bleed
8	CT	17	axial 678x542	0.5x0.5x5 (1-9) 0.5x0.5x10 (10-17)	Frontal astrocytoma high grade glial

but rather a *working coordinate system* XYZ in which X and Y are oriented along the rows and columns of each image slice, and Z is the actual axis of the scan (Figure 2, black coordinate axes). The orientation of the working coordinate system differs from the ideal coordinate system by three rotation angles, *pitch*, *roll* and *yaw*, about the X_0 , Y_0 and Z_0 axes, respectively.

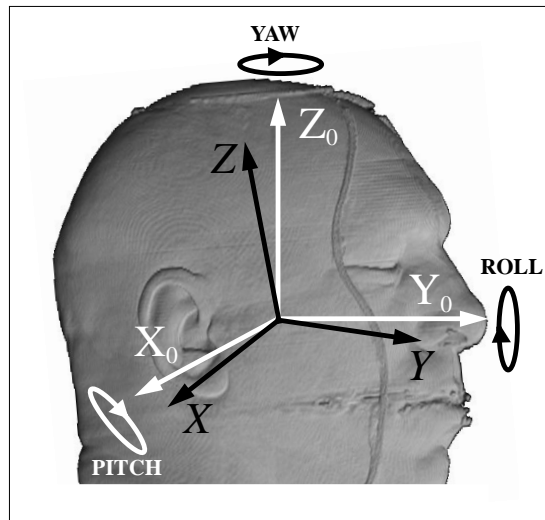


Figure 2. Ideal head coordinate system $X_0Y_0Z_0$ vs. the working coordinate system XYZ. Rendered head courtesy of the Visible Human Project.

2.1. Geometry of the Symmetry Plane

Under the *working coordinate system*, the bilateral symmetry plane can be represented as

$$aX + bY + cZ + d = 0, \quad (1)$$

and the i th axial slice by the plane equation $Z = Z_i$. The symmetry axis (a 2D line) on the i th slice is the intersection of the above two planes:

$$aX + bY + (cZ_i + d) = 0. \quad (2)$$

By examining this line equation, we can make two immediate observations. First, the orientation angle of each 2D symmetry axis, namely $\theta_i = \arctan(b/a)$, should be the same for all slices regardless of their Z_i position. Secondly, the offset $trans_i$ of the symmetry axis on slice $Z = Z_i$ exhibits a simple linear relationship with Z_i , namely

$$trans_i = cZ_i + d \quad (3)$$

from which, given the translational offset of at least two symmetry axes on different slices, we can compute symmetry plane parameters c and d by solving a set of linear equations. These observations form the basis for the symmetry plane extraction algorithm described in the next section.

Further analysis shows how the observable quantities (the 2D symmetry line orientation θ_i and translation $trans_i$ for each axial slice) are related to the 3D pose of the working coordinate system. Under the ideal coordinate system, the 3D orientation of the bilateral symmetry plane is $(1, 0, 0)$. Due to tilting of the patient's head, and an arbitrary decision by the technician as to the pitch angle, points in the ideal coordinate system are reoriented into the observed working coordinate system by an unknown general rotation

$$\begin{aligned} \mathcal{R} &= \mathbf{yaw}(\theta)\mathbf{roll}(\phi)\mathbf{pitch}(\omega) \\ &= \begin{bmatrix} c\phi c\theta & c\theta s\omega s\phi - c\omega s\theta & c\omega c\theta s\phi + s\omega s\theta \\ c\phi s\theta & c\omega c\theta + s\omega s\phi s\theta & c\omega s\phi s\theta - c\theta s\omega \\ -s\phi & c\phi s\omega & c\omega c\phi \end{bmatrix} \end{aligned}$$

where $c\theta \equiv \cos\theta$, $s\theta \equiv \sin\theta$, and so on. This rotation transforms the unit normal of the symmetry plane from $(1, 0, 0)$ to

$$\mathcal{R}(1, 0, 0)^T = (\cos\phi \cos\theta, \cos\phi \sin\theta, -\sin\phi)^T.$$

Thus, the symmetry plane equation can be rewritten in terms of its yaw and roll angles as

$$\cos\phi \cos\theta X + \cos\phi \sin\theta Y - \sin\phi Z + d = 0$$

Matching up our plane parameters a, b, c (Equation (1)) with this equation, we find by inspection that

$$\tan\theta = b/a \quad (4)$$

$$\tan\phi = -c/\sqrt{(a^2 + b^2)}. \quad (5)$$

That is, the shared angle $\theta = \theta_i$ of each axial slice is actually the yaw angle of the head's working coordinate system. Furthermore, the roll angle ϕ is determined by the offsets of the symmetry axes on the set of slices. From equations (3) and (5), when the roll angle ϕ is zero, $c = 0$, and thus $trans_i = d$; otherwise $trans_i$ varies from slice to slice. Finally, the quantity $d/\sqrt{(a^2 + b^2)}$ represents the perpendicular distance of the bilateral symmetry plane from the origin of the working coordinate system, and therefore also represents the offset of the working coordinate system from the origin of the ideal head coordinate system (which lies on the symmetry plane) in the direction normal to the plane.

In summary, if we can extract the 2D axes of reflectional symmetry from a set of axial slices, we can completely determine the the geometric equation $aX + bY + cZ + d$ of the ideal 3D bilateral symmetry plane of the head. Furthermore, we can infer from this equation some of the 3D pose parameters of the patient's head, namely the yaw angle θ , roll angle ϕ and the translational offset from the ideal coordinate system origin along the unit normal direction $(\cos\phi \cos\theta, \cos\phi \sin\theta, -\sin\phi)^T$.

2.2. Symmetry Plane Extraction Algorithm

The geometric results from the previous section have been used to develop an algorithm for automatically detecting the bilateral symmetry plane of a neural brain scan. The input is a set of CT or MR images from an axial (or coronal) brain scan, along with its voxel dimensions. The format of the images we currently receive varies from scanned-in 8-bit gray images, with an average size of 650×550 , to 16-bit DICOM3 format raw images with a standard size of 256×256 . Although both image formats are dominated by the patient's head, the former often contains additional clutter in the form of patient data and acquisition parameters, as well as the physical cross-section of the headrest, superimposed on the slice (Figure 7). We have developed a simple procedure for preprocessing each slice to remove this clutter and thereby isolate just the head region by adaptively thresholding to produce a binarized image, and choosing the largest connected region in that image (details can be found in⁵).

2.2.1. Estimating the Symmetry Axis Orientation $\theta_i \rightarrow \theta$

As indicated in our geometric discussion, each 2D symmetry axis should have the same orientation θ , which also corresponds to the yaw angle of the patient's head. We begin by extracting an estimate of this angle from each 2D axial slice, then combining the measurements to form a single best estimate.

To estimate the orientation θ_i of the 2D symmetry axis of image S_i , representing axial slice $Z = Z_i$, we refer to the definition of bilateral symmetry: a reflection of a bilaterally symmetric image S_i about its symmetry axis produces a figure S'_i that is approximately identical to S_i . We thus search for the orientation of the reflection line that maximizes the cross-correlation between the original image and the rotated, reflected image. First the image S_i is reflected about its vertical center line, to produce a new image $ref_V(S_i)$ (note: this *does not* assume that the symmetry axis is the vertical center line of the image). If the reflection axis of S_i (Figure 3a) is oriented θ degrees from vertical, then the symmetry axis of $ref_V(S_i)$ (Figure 3b) will be oriented $-\theta$ degrees from vertical, regardless of where it appears in the image. Therefore, to evaluate a candidate orientation θ_j within some range, we rotate $ref_V(S_i)$ by $2\theta_j$ about the center of the image, cross-correlate with the original image S_i , and record the maximum correlation value. Formally, the maximum cross-correlation value $C_max_i(\theta_j)$ for brain slice i at angle θ_j can be expressed as $C_max_i(\theta_j) = \max(C_i(\theta_j)(x', y'))$, where

$$C_i(\theta_j)(x', y') = \sum_{x=1}^{x_0} \sum_{y=1}^{y_0} S'_i(x + x', y + y') \times S_i(x, y)$$

and $S'_i = rot(2\theta_j, ref_V(S_i))$, $size(S_i) = size(S'_i) = [x_0, y_0]$, $x' \in [-x_0, x_0]$, $y' \in [-y_0, y_0]$, and $S'_i(x, y) = 0$ when $x < -x_0$, $x > x_0$, $y < -y_0$, or $y > y_0$.

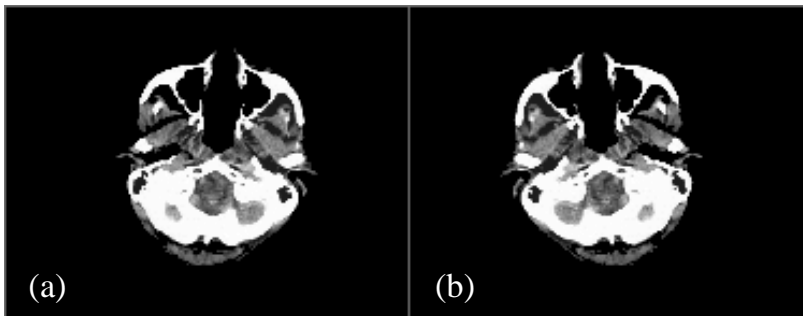


Figure 3. a) A CT axial Head image S_i . b) Vertically reflected image $ref_V(S_i)$.

Recall that the 2D cross-correlation result $C_i(\theta_j)(x', y')$ is a 2 dimensional array double the size of the original image in both X and Y dimensions. Elements in the array contain correlation values for all possible horizontal and vertical disparities between the original image and the rotated reflected image (Figure 4), and thus reflecting S_i about the vertical center line, and rotating $ref_V(S_i)$ about the center of the image before doing cross-correlation, does not miss any possible solutions. That is, our method of computing symmetry axis orientation is invariant to any translation of that axis in the image.

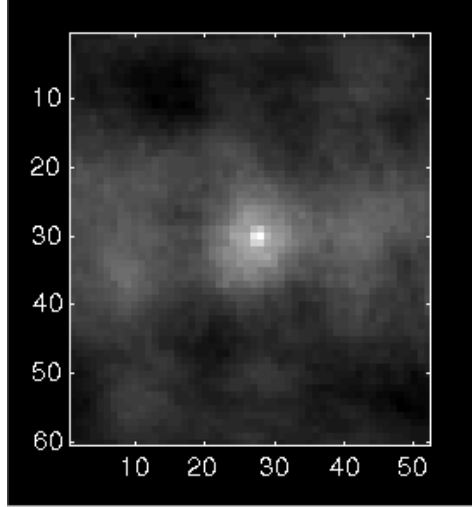


Figure 4. The image of the correlation result: a 2D image where the density of each pixel (x, y) records the correlation score at that relative shifted location of the two images S_i and $rot(2\theta_j, refl_V(S_i))$. The brightest point indicates the highest correlation score.

The maximum value of the cross-correlation surface is evaluated for each θ_j within a range of candidate symmetry axis orientations. For efficiency the actual search is performed in frequency space[†]. That is,

$$\begin{aligned} C_i(\theta_j) &= \max \{ \text{XCorr}(S_i, rot(2\theta_j, refl_V(S_i))) \} \\ &= \max \{ \mathcal{F}^{-1}(\mathcal{F}^*(S_i)rot(2\theta_j, refl_V(\mathcal{F}(S_i)))) \} \end{aligned}$$

where $\mathcal{F}^*(S_i)$ is the complex conjugate of Fourier transform of S_i and \mathcal{F}^{-1} is the inverse Fourier transformation.^{10,11} In most instances a single, well-defined peak occurs in each cross-correlation surface $C_i(\theta_j)$ (Figure 4), as well as in the plot $C_max_i(\theta_j)$ formed by plotting the maximum cross-correlation value for a range of candidate symmetry axis angles θ_j (Figure 5). We choose as an estimate θ_i of the best symmetry axis orientation for slice S_i the value of θ_j that produces the highest peak in the plot of max correlation score vs. angle, that is, $\theta_i = \arg \max(C_max_i(\theta_j))$.

Since all brain slices in the scan should have the same 2D symmetry axis orientation (Equation 2), it is necessary to combine results from each slice to produce a reliable cumulative estimate of the yaw angle θ . Several methods have been tested, falling into two broad categories: either combining the θ_i estimates for each slice, or by combining the cross-correlation vs. angle plots $C_max_i(\theta_j)$ directly. The methods that have been tested are (1) mean value of θ_i over all slices, (2) weighted mean of θ_i , giving the lower slices more weight, (3) median of θ_i , (4) $\arg \max(\sum_i C_max_i(\theta_j))$, that is, the θ_j index of the highest peak in the sum of the cross correlation vs. angle curves for each slice, and (5) same as (4), but after smoothing the cumulative curve with a Gaussian filter. The experiment results show (1) and (2) are almost indistinguishable (less than 0.3 degree difference), and (4) gives the best overall result (Section 2.3).

2.2.2. Determining the Symmetry Plane Equation

Having computed an estimate θ that best describes the shared orientation of each 2D bilateral symmetry axis, we then compute an offset $trans_i$ of the symmetry axis of each slice. Each image S_i is rotated by an angle $-\theta$ so that its symmetry axis should be oriented vertically in the image. That image is then cross-correlated with a vertical reflection of itself taken about the center of the image. The column at which the two produce the highest cross-correlation value is chosen as the value of $trans_i$ for that slice.

Given estimates θ and $trans_i$ for each slice, it is then possible to compute the four parameters of the 3D bilateral symmetry plane (Equation 1). From Equation 2.1, and keeping in mind we can divide all parameters by a constant, we have $a = \cos \theta$ and $b = \sin \theta$. To compute values for symmetry plane parameters c and d , recall that the simple

[†]Note that since the Fourier transform \mathcal{F} commutes with rotations and vertical reflections, we only have to compute the Fourier transformation of S_i once – the flipped and rotated versions can be generated directly in frequency space by flipping and rotating the image $\mathcal{F}(S_i)$.

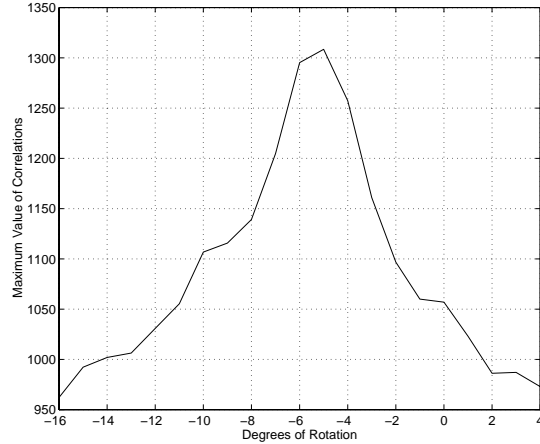


Figure 5. Plot of the maximum cross-correlation, $C_{max_i}(\theta_j)$, between $rot(2\theta_j, ref_V(S))$ and S , for θ_j between -16 and 4 degrees sampled at every 1 degree.

linear relationship (Equation 3) defines an overdetermined set of linear equations in $trans_i$ and Z_i that can be solved for c and d . Solving this linear set of equations is equivalent to fitting a plane to a set of parallel lines in the 3D Euclidean space, each having orientation θ .

As a final step, we recompute the offsets of an optimized symmetry axis on each slice, having orientation θ and $final_trans(i) = c * Z_i + d$. This is equivalent to intersecting the bilateral estimated symmetry plane with each brain slice to obtain a new set of 2D symmetry axes.

2.3. Results and Evaluation

The algorithm has been tested on both CT (enhanced and non-enhanced) and MR (T1,T2, enhanced and non-enhanced) images. Figure 6 shows the final symmetry axis extracted on each input brain slice from Figure 1. Figures 7, 8 and 9 show the extracted symmetry axes under various conditions. Figure 10 shows the symmetry axes extracted from a set of axial images with a roll angle of 15 degrees.

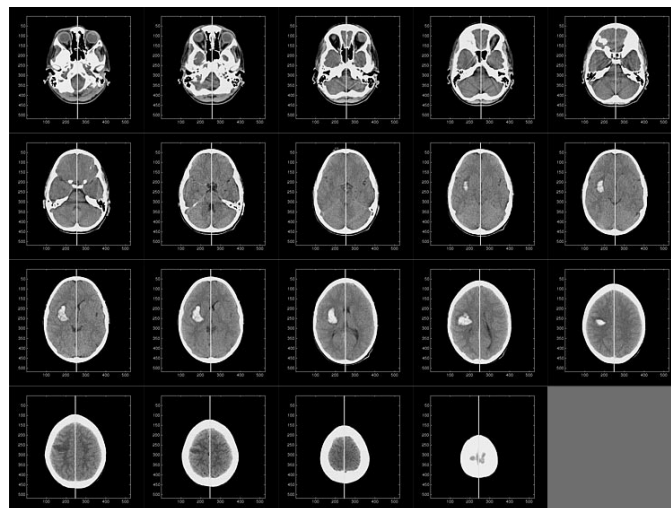


Figure 6. Final symmetry axes superimposed on a set of CT scan slices.

To measure the accuracy of the algorithm, we have a neuroradiologist hand draw the ideal mid line on each 2D slice of several randomly chosen sets of images. The radiologist needs the whole set of images shown for reference while he works on each slice. Figure 11 shows a plot of the angles of symmetry axes chosen by the expert against the

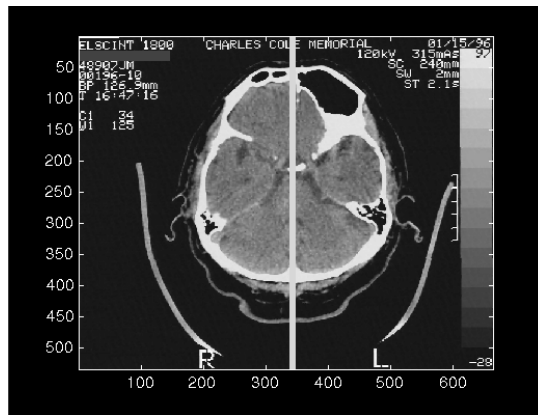


Figure 7. The symmetry axis extracted from a CT scan where obvious asymmetry is present due to a dilated frontal sinus outside of the brain.

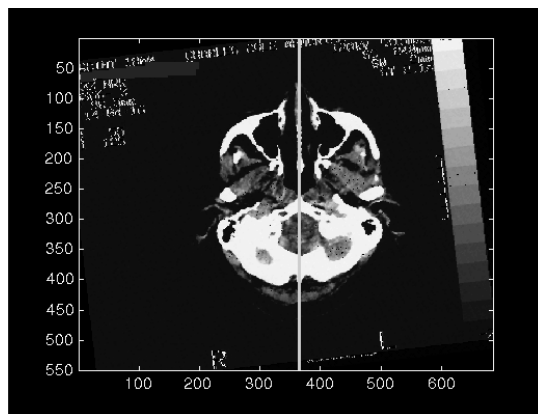


Figure 8. The symmetry axis is extracted and the image is rotated to correct the yaw angle error (-6.5 degree) in the input data.

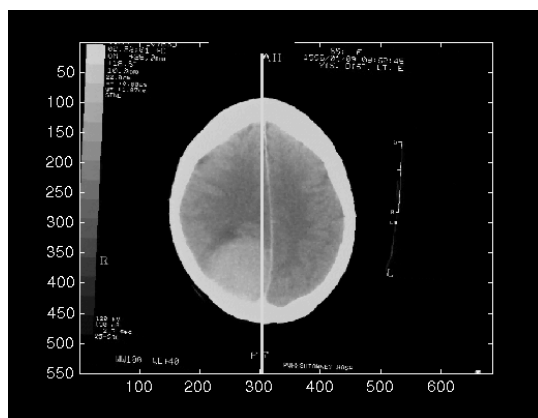


Figure 9. The symmetry axis extracted from a CT scan where obvious asymmetry is present due to a tumor.

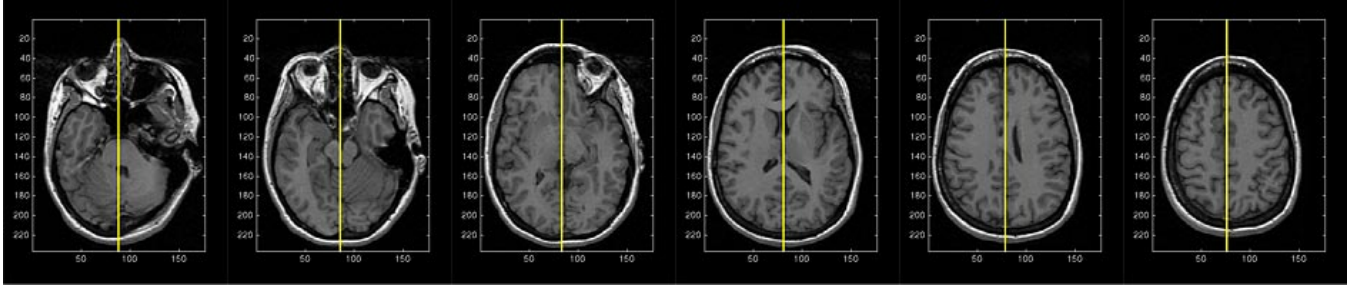


Figure 10. The symmetry axes extracted from a set of axial slices with 15 degree roll angles.

ones computed by our algorithm. Notice that our algorithm provides more accurate values in the lower brain slices, because those slices present more complex bilateral bony structures, in contrast to the slices higher in the brain, which become ovals or even near-circular at the tip of the head. On the contrary, the human expert felt less certain on the lower slices since they lack midline markers as the higher slices do. Although theory tells us the yaw angle of the symmetry axes on each axial slice should be the same, there is a measurement variation in the yaw angles determined by the human expert. The standard deviations on different sets of slices vary from 0.6 to 1.8 degrees. In all cases, the difference between the mean value of the human picked yaw angles and the algorithm detected yaw angle is less than one degree. For this kind of accuracy, the initial rotational errors in the images can be as large as near 90 degrees.

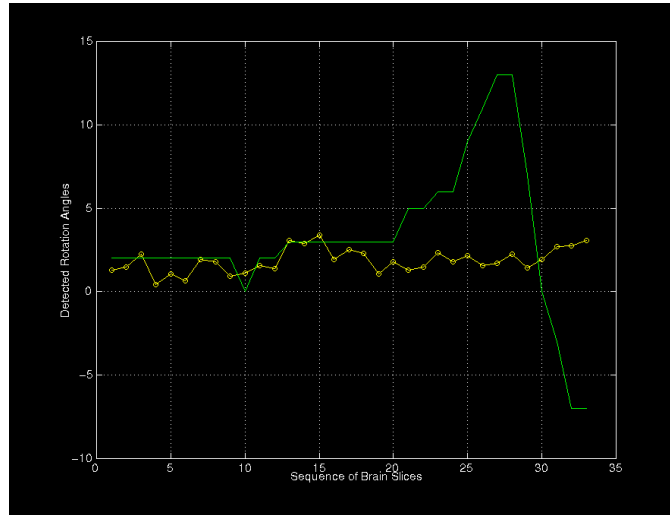


Figure 11. The angles of the symmetry axes chosen by a neuroradiologist (curve with dots) versus the angles, $\theta_i = \arg \max(C_max_i(\theta_j))$, computed by our algorithm. This is dataset (3) of Table 1. The algorithm determined angle is 2 degrees, the mean of the expert chosen angle is 1.9 degrees with standard deviation 0.7 degrees.

To evaluate the accuracy of computed roll and yaw angles, a densely sampled MR image set was resampled using trilinear interpolation to artificially vary the yaw angles from -10 to 10 degrees in 2.5 degree intervals, and the roll angles from -15 to 15 degrees in 5 degrees intervals. Figure 12 shows a set of coronal slices with varying roll angles (Figure 12).

The average accuracy of the algorithm on both yaw and roll angle detection is under one degree (< 0.3 degrees for the yaw angles and < 0.75 degrees for the roll angles), after taking into account the nonzero yaw angle of 1.25 degrees and roll angle of -1.75 in the original dataset (Figure 13, Figure 14). Given the sample interval for finding the symmetry axis on each slice is one degree, this result is excellent.

Given a volumetric brain scan, our algorithm can identify the errors in yaw and roll angles in the input data, and correct these errors by recutting the input volume. The final result is an automatically extracted “midsagittal”

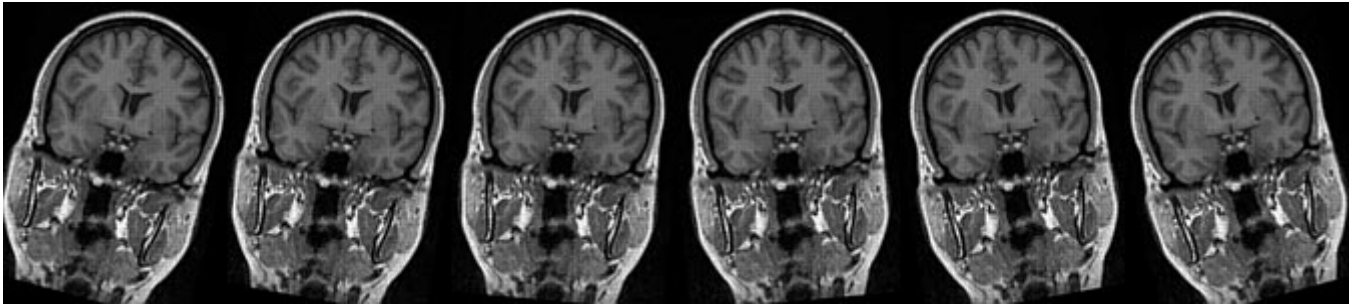


Figure 12. One slice sample from the coronal input with varied roll angles.

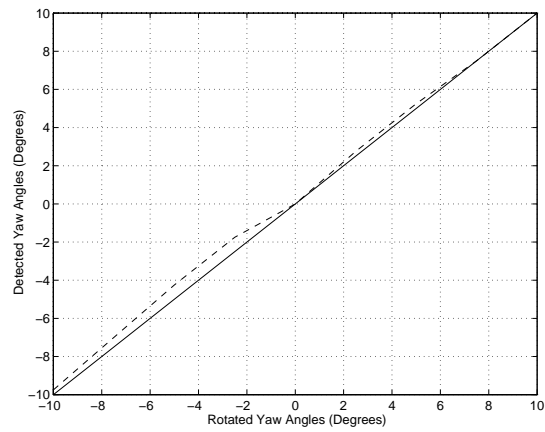


Figure 13. Actual vs detected yaw angles in the MR original axial scans. The solid line is the perfect detection result and the dashed line is formed from the detected yaw angle values using our algorithm.

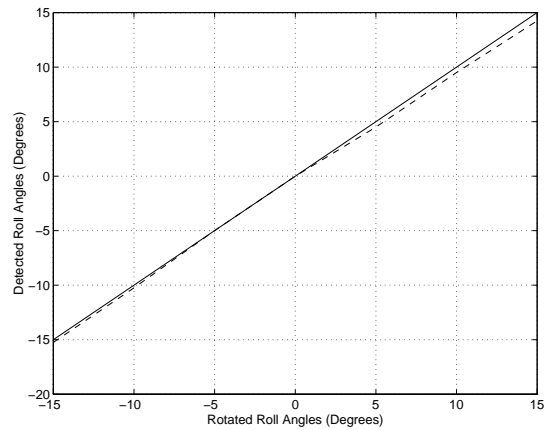


Figure 14. Actual vs detected roll angles in the MR resliced coronal scans. The solid line is the perfect detection result and the dashed line is formed from the detected roll angle values using our algorithm.

image representing densities occurring on the bilateral symmetry plane (Figure 15).

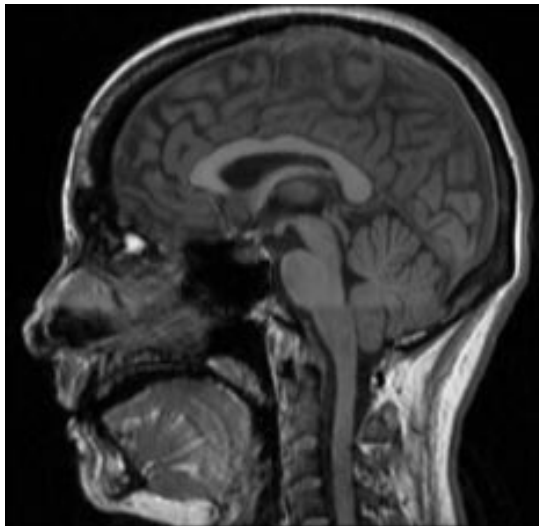


Figure 15. The mid-sagittal plane automatically extracted from the MR data set (Table 1, data set (4)). The detected yaw is 1.25 degrees and the detected roll angle is -1.75 degrees.

We have observed that our symmetry axes computation is not adversely affected by lesions and mass effects in the images. The bony skull is influential, but the accuracy of the detected symmetry axes decreases when the symmetry axes are determined by the silhouette of an axial or coronal brain slice alone. The internal structure of the brain thus appears to enhance the position and orientation accuracy.

In the higher brain slices, a thin membrane that separates the two hemispheres of the brain is visible as a thin (1-3 pixel wide) linear feature in the image. In the ideal case, this membrane should line up exactly with the centerline computed using symmetry detection (compare Figures 1 and 6). However, in real examples, the membrane may appear to be displaced from the computed centerline, due to 1) inaccuracies in the computed centerline, and 2) physical displacement of the membrane due to the mass effect caused by tumors or bleeds in the brain. Extracting the actual position of this membrane from image data can be used in the former case to refine the computed centerline estimate, and in the latter case to provide a quantitative measure of mass effect.

3. DISCUSSION AND CONCLUSIONS

When a set of axial slices has a large roll angle error, the actual medial line of the brain is shifted off from the symmetry axis of the whole image. We have applied the symmetry axis extraction algorithm to sets of reinterpolated coronal slices in these situations, to estimate the roll angles and achieved accurate results as shown in Section 2.3.

The general contribution of this work is a simple idea: if a set of objects (human brains) are known to be approximately symmetrical, we can use the symmetry's invariance (midsagittal plane) as a computational guidance for segmentation, inter-subject registration, and screening. We have carried out this idea in neuroradiological image understanding by developing an effective mid-sagittal plane extraction algorithm that works using clinical, multi-modality, cluttered, sparse, partial, normal and pathological brain image data; and various applications derived from its results, including: automatic lesion detection, mass effect quantification, and brain/atlas alignment.^{5,6} The robustness and simplicity in this approach resides in the fact that the image understanding process is not limited to information provided by low-level image data alone, but is guided by the intended symmetry as well.

This work successfully combines 2D and 3D images in such a way that 2D data is used to predict a 3D plane (roll angles) and the 3D image is used to correct local errors in the 2D slices. The estimated head rotation angles are within one degree of rotational accuracy as compared with human experts (neuroradiologists).

In summary, our work deals with pathological clinical 3D images, which can exhibit severe asymmetries. Our approach not only identifies symmetry axes where they exist (in normal brains), but where they are supposed to exist

(in pathological brains). Our work presents a sound geometric method for estimating the symmetry of a 3D object using a sparse set of 2D slices. Little work has been reported on effective approaches dealing with sparsely-sampled sets of clinical images and/or pathological cases, both of which are of great importance in applied medical image analysis. Finally, we have extensively tested the algorithm, and have evaluated its relative accuracy with respect to “ground truth” data from a human expert.

Our current work includes further evaluation of inter-subject gross registration results in terms of those parameters other than the yaw, roll angles and translation along the X axis, determination of the anatomical location of a detected lesion, comparisons of different brain lesions in 3D and effective indexing of a 3D brain image for retrieval.

Acknowledgements

This research is sponsored by the Allegheny-Singer Research Institute under prime contract through the National Institute of Standards and Technology (NIST#70NANB5H1183). Views and conclusions contained in this document are those of the authors and should not be interpreted as necessarily representing official policies or endorsements, either expressed or implied, of the National Institute of Standards and Technology or the United States Government.

REFERENCES

1. P. Allain, J.M. Travère, J.C. Baron, and D. Bloyet. *Quantification of Brain Function. Tracer Kinetics and Image Analysis in Brain PET: Accurate PET positioning with reference to MRI and neuroanatomical data bases*, pages 401,408. Elsevier Science Publishers, B.V., 1993.
2. R. Bajcsy and S. Kovacic. Multiresolution elastic matching. *Computer Vision, Graphics, and Image Processing*, 46:1–21, 1989.
3. C. Davatzikos. Nonlinear registration of brain images using deformable models. In *Proceedings of the workshop on Mathematical Methods in Biomedical Image Analysis*, pages 94,103. IEEE Computer Society, June 1996.
4. P.J. Flynn. 3D Object Recognition with Symmetric Models: Symmetry Extraction and Encoding. *IEEE trans. on Pattern Analysis and machine Intelligence*, to appear.
5. Y. Liu, R.T. Collins, and W.E. Rothfus. Automatic extraction of the central symmetry (mid-sagittal) plane from neuroradiology images. *Carnegie Mellon University, The Robotics Institute Technical Report*, (96-40):1:29, November 1996.
6. Y. Liu, W. Rothfus, and T. Kanade. Content-based 3d neuroradiologic image retrieval: Preliminary results. *IEEE International Workshop on Content-Based Access of Image and Video Databases, CAIVD'98, Volume=IEEE Computer Society, Number=Bombay, India, Month=January, Year=1998, Pages=91,100*.
7. F. Maes, A. Collignon, D. Vandermeulen, G. Marchal, and P. Suetens. Multimodality image registration by maximization of mutual information. *IEEE Transactions on Medical Imaging*, 16(2):187,198, 1997.
8. T. Masuda, K. Yamamoto, and H. Yamada. Detection of partial symmetry using correlation with rotated-reflected images. *Pattern Recognition*, 26(8):1245,1253, 1993.
9. M Moshfeghi. Elastic matching of multimodality medical images. *CVGIP:Graphical Models and Image Processing*, 53:271–282, 1991.
10. A. Rosenfeld and A.C. Kak. *Digital Picture Processing*. Academic Press, New York, 1976.
11. John C. Russ. *The Image Processing Handbook*. CRC Press, Boca Raton, Ann Arbor, London, Tokyo, 1992.
12. C. Studholme, D.L.G. Hill, and D.J. Hawkes. Automated 3-d registration of MR and CT images of the head. *Medical Image Analysis*, 1(2):163–175, June 1996.
13. J. Talairach and P. Tournoux. *Co-Planar Stereotaxic Atlas of the Human Brain*. Thieme Medical Publishers, 1988.
14. J.P. Thirion. Fast intensity-based non-rigid matching. In *Proc. of 2nd Intl. Symp. on Med. Robotics and Comp. Ass. Surgery*, pages 47–54, 1995.
15. P. Viola and W. Wells III. Alignment by maximization of mutual information. In *ICCV95*, pages 16–23, 1995.
16. R. Waltzman. Finding symmetries of polyhedra. Technical Report CAR-TR-333, CS-TR-193, Center for Automation Research, University of Maryland, College Park, MD., 1987.
17. W.M. Wells III, P. Viola, H. Atsumi, S. Nakajima, and R. Kikinis. Multi-modal volume registration by maximization of mutual information. *Medical Image Analysis*, 1(1):35–51, March 1996.
18. J.D. Wolter, T.C. Woo, and R.A. Volz. Optimal algorithms for symmetry detection in two and three dimensions. In *The Visual Computer*. Springer-Verlag, New York, 1985.